Food Science of Animal Products

Research Article

Genome sequence and metabolic analysis of *Pseudomonas fragi* unveil the meat spoilage and CO_2-antibacterial mechanism under high-oxygen modified atmosphere packaging

Jun Yang[1,2], Yikun Xu[1], Yimin Zhang[1,2], Rongrong Liang[1,2], Lixian Zhu[1,2], Yanwei Mao[1,2], Xin Luo[1,2], Xiaoyin Yang[1,2] ✉

[1] *Laboratory of Meat Processing and Quality Control, College of Food Science and Engineering, Shandong Agricultural University, Tai'an 271018, China*

[2] *National R&D Center for Beef Processing Technology, Tai'an 271018, China*

✉Address correspondence to Xiaoyin Yang, yangxiaoyin@sdau.edu.cn

Received: August 30, 2024; Revised: September 21, 2024; Accepted: September 29, 2024

Abstract: *Pseudomonas fragi* is a predominant meat-borne spoilage bacterium that is sensitive to CO_2 under high-oxygen modified atmosphere packaging (HiOx-MAP). This study was designed to reveal the spoilage potential of a popular wild-type *P. fragi* T1 in HiOx-MAP beef by whole genome sequencing, and explore the bacterial metabolic response to CO_2 utilizing combined metabolomic and volatile organic compounds (VOCs) analysis, under treatment (CO_2-enriched) HiOx-MAP (TMAP, 50% O_2/40% CO_2/10% N_2) or control (non-CO_2) HiOx-MAP (CMAP, 50% O_2/50% N_2) during chilled storage. Results showed that the strain *P. fragi* T1 was endued with spoilage-related genes associated with protease, lipase and esterase production, amino acid metabolism, carbon metabolism, sulfur metabolism, and putrescine metabolism, which was responsible for the hydrolysis of meat protein and lipid, as well as off-odor formation. The growth of *P. fragi* under CMAP resulted in the production of VOCs, such as diacetyl, 1-undecene, 2-undecanone, nonanal, (*Z*)-5-decen-1-ol, and (*E*)-2-octenal, etc. The TMAP declined above VOCs concentrations significantly ($P < 0.05$) by inhibiting *P. fragi* growth and regulating its metabolic activities. The metabolomic analysis further manifested that CO_2 inhibited the *P. fragi* growth by decreasing cell membrane fluidity, disturbing energy metabolism, and inhibiting amino acid metabolism and nucleotide biosynthesis. This work provides valuable information for understanding the *P. fragi*-induced meat spoilage phenomena, and the antibacterial mechanism of CO_2 against *P. fragi*.

Keywords: *Pseudomonas fragi*; CO_2 antibacterial mechanism; metabolomics; whole genome sequence; volatile organic compounds

Citation: J. Yang, Y. K. Xu, Y. M. Zhang, et al., Genome sequence and metabolic analysis of *Pseudomonas fragi* unveil the meat spoilage and CO_2-antibacterial mechanism under high-oxygen modified atmosphere packaging, Food Sci. Anim. Prod. 2 (2024) 9240084. https://doi.org/10.26599/FSAP.2024.9240084.

1 Introduction

Beef is a nutrient-rich foodstuff excelling in moisture, protein, vitamins, and minerals, nevertheless, the nutrient-rich condition meanwhile provides the optimal conditions for the growth of specific spoilage organisms (SSOs), such as *Pseudomonas*, Enterobacteriaceae, and *Brochothrix thermosphacta*[1–2]. The reproduction of SSOs leads to a number of unfavorable outcomes, including meat discoloration, unacceptable off-odor production, slime and softening, therefore, meat products are ultimately rejected by consumers[3–4]. Among them, *Pseudomonas fragi* has been well-known as a pivotal spoiler in limiting beef shelf-life due to its strong proteolytic and lipolytic activities, as well as its production of spoilage metabolites[5–6]. Although the *P. fragi* spoilage behaviors are largely genetically determined[7–8], there is a paucity of bioinformatics studies that have investigated the genetic characteristics of meat-borne *P. fragi* with respect to its spoilage potential.

High-oxygen modified atmosphere packaging (HiOx-MAP) has been developed into a worldwide packaging system to extend meat shelf-life due to the excellent CO_2-antibacterial effect[3,9]. Compared to the common HiOx-MAP (80% O_2/20% CO_2), an elevated CO_2 level to 40% on the basis of declining O_2 level to 50% (50% O_2/40% CO_2/10% N_2) not only demonstrated a distinguished antibacterial impact on Gram-negative bacteria (e.g., *Pseudomonas* and Enterobacteriaceae), but also exhibited tremendously inhibitory activity against Gram-positive bacteria[9]. As reported, *P. fragi* is the most sensitive species to CO_2 in HiOx-MAP beef[2]. It is known that CO_2 plays an important role in microbial metabolic processes. For instance, CO_2 can serve as the biosynthetic substrate for the carboxylation reaction or as the metabolic product of the decarboxylation reaction, and CO_2 is also capable of affecting the rate of some certain bacterial enzymatic reactions, making changes to the concentrations of targeted metabolites[10–11]. Oliver et al.[12] reported that CO_2 inhibited the synthesis of *Streptococcus diacetilactis* decarboxylase. King et al.[13] and Tan et al.[14] found that CO_2 caused an observable block in both *P. aeruginosa* and *P. fluorescens* metabolism as evidenced by a decreased isocitrate dehydrogenase and malate dehydrogenase activity. Nevertheless, the regulatory effect of CO_2 on *P. fragi* intracellular metabolic activity with respect to meat spoilage remains poorly understood, and its precise bacteriostatic targets or mechanism are worth further elucidating. Metabolomics is recently emerged as a powerful

tool to study intracellular biological and chemical alterations in *P. fragi* under some antibacterial conditions (e.g., 3-carene and linalool)[15–16], which is expected to facilitate our understanding of CO_2-antibacterial mechanism on *P. fragi*.

The dynamic alterations in volatile organic compounds (VOCs) during meat storage are regarded as potential biomarkers indicating meat spoilage process, which are closely linked to bacterial intercellular metabolic actives, such as glucose metabolism and amino acid metabolism[17–18]. Albeit many studies reported several typical VOCs (e.g., ethyl acetate, ethyl hexanoate, ethyl 2-butenoate, 1-octen-3-ol, 2-ethyl-1-hexnaol, 3-methyl-butanal, nonanal, and decanal) produced from *P. fragi*[5,7–8], few have investigated the inner relationship between *P. fragi* metabolic pathways and volatile profiles under HiOx-MAP, especially for the influence of CO_2 on *P. fragi* metabolic regulation and the relevant VOCs formation. In this work, the integration of whole genome mining of a representative wild-type *P. fragi* T1 isolated from HiOx-MAP spoiled beef was conducted to facilitate the deciphering of the *P. fragi* spoilage mechanism. Furthermore, in order to comprehensively demonstrate the *P. fragi* global metabolic regulation after exposure to CO_2, both metabolomics and VOCs produced from *P. fragi* were analyzed during the storage of HiOx-MAP with various CO_2 levels.

2 Materials and methods

2.1 Genomic characteristics of *P. fragi*

2.1.1 Strain and sample preparation

P. fragi T1 strain, with the strongest spoilage potential, was isolated from HiOx-MAP beef steaks after being stored for 20 d[2]. This strain has been used for investigating the effect of CO_2 on *P. fragi* spoilage behavior[8]. For genomic sample preparation, *P. fragi* T1 was firstly cultured in brain heart infusion (BHI) broth (Beijing Land Bridge Technology Co., Ltd., Beijing, China) at 28 °C (200 r/min) for 24 h. Subsequently, *P. fragi* cells were harvested and washed three times by centrifugation (5 000 × *g*, 5 min) in phosphate-buffered saline (PBS, pH 7.4), and the culture pellets were then frozen in liquid nitrogen and stored at −80 °C prior to DNA extraction.

2.1.2 Genome sequencing, assembly, and annotation

The genomic DNA of *P. fragi* T1 was extracted by the genomic DNA extraction kit (Tiangen Biotech Co., Ltd., Beijing, China), and genome sequencing was performed using Oxford Nanopore Technologies (ONT) at Biomarker Technologies (Beijing, China). After sequencing, the reads of adapters, low-quality and short fragments (length < 2 000 bp) were first filtered, and the reads were then assembled using Canu v1.5 software. The third generation reads were used to correct the assembly results with Racon v3.4.3. Then, Circlator v1.5.5 software was used to circularize and adjust the starting site, followed by further correction using the second-generation data from Pilon v1.22 software to collect genomic information with higher precision. For genome component prediction, coding genes prediction was performed by Prodigal v2.6.3. The GenBlastA v1.0.4 program was used to scan the whole genomes after masking predicted functional genes. Putative candidates were then analyzed by searching for non-mature mutations and frame-shift mutations using GeneWise v2.2.0. Transfer RNA (tRNA) genes, ribosome RNA (rRNA) genes, and repetitive sequences were predicted with tRNAscan-SE v2.0, Infernal v1.1.3, and RepeatMasker v4.0.5, respectively. Additionally, the genomic map of *P. fragi* was visualized using Circos v0.66. Functional annotation was performed using the evolutionary genealogy of genes: Non-supervised Orthologous Groups (eggNOG) database, Gene Ontology (GO) database, Kyoto Encyclopedia of Genes and Genomes (KEGG) database, National Center of Biotechnology Information (NCBI) Non-redundant Protein (NR) database, Protein families (Pfam) database, Swiss-Prot database, and TrEMBL database to obtain the corresponding annotation information.

2.2 Storage experiment

The *M. longissimus lumborum* muscles (loins) were obtained from the left side of three carcasses of Simmental × Luxi crossbred bulls (24 months old, $pH_{48\,h}$ = 5.55–5.65) at a local commercial abattoir after a chilling (2–4 °C) for 48 h. All loins were then transferred to the lab on ice to produce beef juice, in accordance with the methodology described by Illikoud et al.[17].

P. fragi T1 was cultured in accordance with the methodology outlined in section 2.1.1 and Yang et al.[8]. Afterwards, the *P. fragi* T1 cultures were diluted with precooled PBS (pH 7.4) to achieve 8 (lg (CFU/mL)), and 1 mL suspension was then inoculated into prepared beef juice (1 L), resulting in an initial colony count of 5 (lg (CFU/mL)). Meanwhile, 1 mL sterile 0.85 g/100 mL physiological saline was introduced into beef juice (1 L) to serve as blank control. Subsequently, 10 mL of beef juice was transferred to a 25 mL glass vial, and 4 glass vials were placed in a polypropylene tray (TQBC-0775, Sealed Air Co., Danbury, USA). All trays were randomly subjected to the treatment HiOx-MAP (TMAP, 50% O_2/40% CO_2/10% N_2) or the control HiOx-MAP (CMAP, 50% O_2/50% N_2) using a DT-6D MAP machine (Dajiang Machinery Equipment Co., Ltd., Nanjing, China). All packaging were then stored in a dark chiller (4 °C) for 12 d. On days 0, 1, 2, 3, 4, 5, 6, 7, 8, 10, and 12, enumeration of the *P. fragi* colony was conducted to establish the growth curve. VOCs of beef juice were detected on days 0, 1, 4, 8, and 12, and intracellular metabolome analysis of *P. fragi* was conducted on days 1 and 8, according to the growth curve. Six biological replications were performed for the analysis of colony enumeration, VOCs, and metabolomics.

2.3 VOCs analysis

The beef juice samples were removed from the refrigerator at −80 °C and quickly thawed under running water. Then VOCs were immediately extracted using a headspace solid-phase micro-extraction (HS-SPME). Briefly, beef juice (5 mL) of each sample, NaCl (1 g), and internal standard (10 μL, 4-methyl-1-pentanol, in vial concentration 1 000 μg/L) were placed in a 20 mL headspace vial, and capped. The headspace vial was incubated at 37 °C for 10 min with continuous shaking until the NaCl dissolved. After equilibration at 37 °C for 20 min, VOCs were extracted with an aging SPME fiber assembly 50/30 μm DVB/CAR/PDMS (Supelco, Bellefonte, PA, USA) at 37 °C for 30 min. Subsequently, the fiber was removed from vials and inserted immediately into the gas chromatograph injection port to desorb volatiles at 250 °C for 5 min. Then VOCs were separated using a gas chromatography-mass spectrometry (GC-MS, QP-2010 Plus, Shimadzu, Kyoto, Japan) system as described by Yang et al.[4]. The identification of VOCs was performed by comparing mass spectrum fragment with the National Institute of Standards and Technology (NIST) 11 library. The concentrations of detected VOCs were semi-quantified using an internal standard methodology (expressed as μg/L).

2.4 Metabolome analysis

2.4.1 Sample preparation and extraction of intracellular metabolites

P. fragi cells were initially harvested and washed three times by centrifugation (5 000 × *g*, 4 °C) for 10 min in precooled PBS (pH 7.4). The cell pellets were rapidly frozen in liquid nitrogen and stored at −80 °C. *P. fragi* samples were ground in liquid nitrogen, and 200 μL of precooled water and 800 μL mixture of precooled methanol and acetonitrile (1:1, *V*/*V*) was added, then the mixture was placed for 20 min ultrasonic shaking in the ice bath. Subsequently, the mixture was placed at −20 °C for 1 h and centrifuged at 16 000 × *g* for 20 min at 4 °C. The supernatant was dried using a high-speed vacuum enrichment centrifuge (Eppendorf, Hamburg, Germany). Subsequently, the resulting powder was redissolved with 100 μL of 50% methanol (*V*/*V*), vortexed, and centrifuged at 20 000 × *g* for 20 min at 4 °C. Then the supernatant was immediately collected and used for metabolomic analysis.

2.4.2 Ultra-high performance liquid chromatography-tandem mass spectrometry (UPLC-MS/MS) analysis

Metabolomics profiling was performed using a UPLC-electrospray ionization (ESI)-Q-orbitrap-MS system (Nexera X2 LC-30AD, Shimadzu, Japan) coupled with Q-Exactive (QE) Plus (Thermo Fisher Scientific, San Jose, CA, USA). For liquid chromatography separation, 8 μL of supernatant was injected and analyzed using an ACQUIY UPLC® HSS T3 column (2.1 mm × 100 mm, 1.8 μm, Waters, Milford, MA, USA). The flow rate was 0.3 mL/min, and the mobile phase A was 0.1% formic acid in aqueous solution, and mobile phase B was 100% acetonitrile. The gradient was 0% mobile phase B for 2 min, and was linearly increased to 48% at 4 min, and then increased to 100% at 4 min and maintained for 2 min, followed by a linear reduction to 0% mobile phase B over 0.1 min, and finally maintained for 2.9 min. Both ESI positive and negative mode were applied for MS data acquisition. The ESI source conditions were set as follows: the spray voltage was set at 3.8 kV for the positive model and −3.2 kV for the negative model, with a sheath gas set at 30 arb. The capillary temperature was 320 °C. For full scans, the analyzer covered a mass range of *m*/*z* 70–1 050, achieving a mass resolution of 70 000. The high energy collision dissociation scan was employed for data-dependent MS/MS acquisition, with normalized collision energy set as 20, 30, and 40 eV. Additionally, quality control (QC) samples were prepared by pooling aliquots of all samples and used for data normalization. Blank samples (75% acetonitrile in water) and QC samples were injected every six samples during acquisition.

2.4.3 Data processing and filtering

The raw MS data were processed using MS-DIAL for peak alignment, retention time correction, and peak area extraction. The metabolites were identified by accuracy mass (mass tolerance < 10^{-5} Da) and MS/MS data (mass tolerance < 0.02 Da) that were matched with the Human Metabolome Database, MassBank, other public databases, and Bioprofile self-built metabolite standard library. The extracted-ion features were filtered, and only the variables having more than 50% of the nonzero measurement values in at least one group were kept.

2.4.4 Multivariate statistical analysis

The alternations in the metabolic profile were examined using orthogonal partial least squares-discriminant analysis (OPLS-DA) by R package. The discriminating metabolites were obtained using a statistically significant threshold of variable importance in the projection (VIP) values obtained from the OPLS-DA model and two-tailed Student's *t*-test (*P* value) on the normalized raw data at univariate analysis level. The *P* value was calculated by one-way analysis of variance for multiple groups analysis. Fold change (FC) was calculated as the logarithm of the average mass response (area) ratio between two arbitrary classes. Metabolites with VIP > 1.0, FC > 2, and $P < 0.05$ were considered to be differentially expressed metabolites (DEMs). In order to analyze the perturbed biological pathways, KEGG enrichment analyses were carried out with the Fisher's exact probability test, and false discovery rate correction for multiple testing was performed. Enriched KEGG pathways were nominally statistically significant at $P < 0.05$.

2.5 Statistical analysis

Statistical analysis for VOCs was performed using the MIXED procedure (SAS, version 9.2) with packaging groups, storage time, inoculation types, and their interaction fitted as fixed factors, and the random factor was packaging replications. Least square means were separated by using the PDIFF option and were considered significant at $P < 0.05$. The heatmap of VOCs and a Spearman correlation analysis were conducted to estimate the relationship between intercellular DEMs and VOCs using R software (version 3.5.1), based on their concentrations.

3 Results and discussion

3.1 Whole genome sequence analysis of *P. fragi*

3.1.1 Genome properties

The whole genome sequencing of *P. fragi* T1 was 5 253 243 bp, with an average GC content of 58.08% (Figure 1A). Non-coding RNA (ncRNA) were identified as tRNA (79), 5S rRNA (9), 16S rRNA (8), and 23S rRNA (8) (Table 1). The genome of *P. fragi* T1 contained 4 757 coding sequences, which was annotated in eggNOG (4 106), GO (3 603), KEGG (2 699), NR (4 720), Pfam (4 142), Swiss-Prot (3 018), and TrEMBL (4 714).

Table 1 Gene prediction and annotation summary of *P. fragi* T1.

Item	Result
Gene number	4 757
Gene total length (bp)	4 627 302
Gene average length (bp)	972
GC content (%)	58.08
Maximum length (bp)	10 251
Minimum length (bp)	90
tRNA number	79
5S rRNA number	9
16S rRNA number	8
23S rRNA number	8

3.1.2 Functional annotation

Most of the genes were involved in eggNOG classification related to amino acid transport and metabolism, transcription, inorganic ion transport and metabolism, energy production and conversion, cell wall/membrane/envelope biogenesis, and signal transduction mechanisms (Figure 1B).

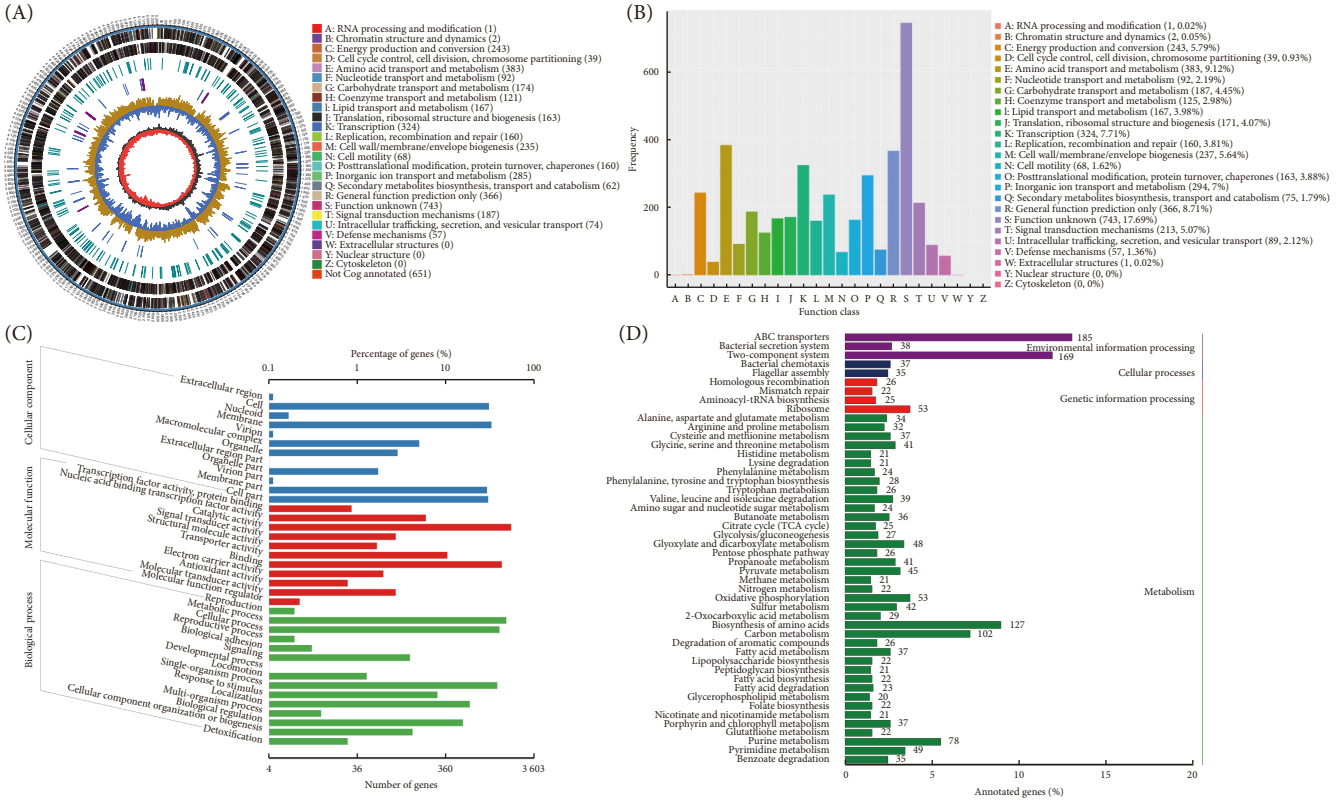

Figure 1 (A) Circular genome map of *P. fragi* T1 and functional annotation of the *P. fragi* T1 genome using (B) eggNOG, (C) GO, and (D) KEGG database. In the circular genome map, the outermost circle of the circle diagram is the marker of genome size, and each scale is 0.5 Mb; the second and third circles are coding DNA sequence (CDS) on the positive and negative chains, respectively. Different colors indicate the functional classification of different clusters of orthologous groups of proteins (COGs) of CDS. The fourth circle is repetitive sequences, the fifth circle is rRNA (purple color) and tRNA (blue color), and the sixth circle is GC content. The outward yellow part indicates that the GC content in this region is higher than the average GC content in the whole genome. A higher peak value indicates a greater difference between the GC content in this region and the average GC content. The inside blue part indicates that the GC content in this region is lower than the average GC content in the whole genome. The innermost circle is the GC-skew value. The color dark gray is used to indicate areas where the value of G is greater than that of C, and the color red is used to indicate areas where the value of C is greater than that of G.

A total of 3 603 genes of *P. fragi* T1 was assigned to GO terms, in which biological process (BP) were the most abundant, followed by cellular component (CC) and molecular function (MF) (Figure 1C). The two most abundant BP categories were metabolic process (1 754 genes) and cellular process (1 468 genes), followed by single-organism process (1 388 genes), localization (677 genes), and biological regulation (566 genes). Among the CC functions, the annotation function with the highest number of genes was membrane (1 192 genes), and cell (1 115 genes) exhibited the second highest gene number. The majority of MF-related genes were found to be associated with catalytic activity (1 992 genes), binding (1 561 genes), transporter activity (377 genes), and nucleic acid binding transcription factor activity (215 genes) in proper order.

The KEGG annotation demonstrated that metabolism contained the most genes, followed by environmental information processing, genetic information processing, and cellular processes (Figure 1D). In the metabolism category, biosynthesis of amino acids (127 genes), carbon metabolism (102 genes), and purine metabolism (78 genes) were enriched, respectively. During environmental information processing, ATP-binding cassette (ABC) transporters and two-component systems were the top 2 pathways (with 185 and 169 gene annotations, respectively), which may promote *P. fragi* environmental self-adaptation and enhance its defense ability against CO_2. Additionally, genes encoding acid stress chaperone HdeA and universal stress protein UspA were detected. In the classification of cellular processes, bacterial chemotaxis (37) and flagellar assembly (35) showed similar gene numbers, and they were related to bacterial physiology involving in motility, growth, nutrient acquisition, and biofilm formation, etc.[19].

3.1.3 *Spoilage-related metabolic pathways*

P. fragi is a robust proteolytic bacterium, whose growth could contribute to the increase in meat pH and total volatile basic nitrogen (TVB-N) content[8,20]. This study identified genes participating in the proteolysis process, including zinc protease, serine protease SohB and DegS (Table 2). Thereinto, the characteristics of serine protease have been researched in *Aeromonas* and *Shewanella*[21–22], but the role of serine protease produced from *P. fragi* in protein degradation of meat remains poorly understood.

Given that genes related to triacylglycerol lipase and glycerophosphoryl diester phosphodiesterase were identified in the present study (Table 2), the *P. fragi* T1 is also able to produce lipase and esterase, which is responsible for hydrolyzing meat fats, and further forming some fruity off-odor associated with short-chain fatty acid ethyl esters[5].

As previously stated in section 3.1.2, amino acid metabolism and carbon metabolism represented the two primary functions of *P. fragi* T1 in KEGG annotations. Both metabolisms could intensify the formation of some off-odor volatiles (e.g., acetate, acetoin, diacetyl, acetic acid, and butanoic acid, etc.), as reviewed by Casaburi et al.[18]. Be that as it may, further investigation into the

Table 2 Spoilage-related pathways and genes of *P. fragi* T1 by KEGG analysis.

Function	KO	KO function	Enzyme
Proteolysis process	K07263	Zinc protease	EC:3.4.24.-
	K04774	Serine protease SohB	EC:3.4.21.-
	K04691	Serine protease DegS	EC:3.4.21.-
Glycerophospholipid metabolism/ glycerolipid metabolism	K01126	Glycerophosphoryl diester phosphodiesterase	EC:3.1.4.46
	K01046	Triacylglycerol lipase	EC:3.1.1.3
Biosynthesis of amino acids	K00620	Glutamate *N*-acetyltransferase/amino-acid *N*-acetyltransferase	EC:2.3.1.35/2.3.1.1
	K01620	Threonine aldolase	EC:4.1.2.48
	K01752	*L*-serine dehydratase	EC:4.3.1.17
	K01478	Arginine deiminase	EC:3.5.3.6
	K01585	Arginine decarboxylase	EC:4.1.1.19
	K01438	Acetylornithine deacetylase	EC:3.5.1.16
	K00930	Acetylglutamate kinase	EC:2.7.2.8
	K01581	Ornithine decarboxylase	EC:4.1.1.17
	K00928	Aspartate kinase	EC:2.7.2.4
	K00789	*S*-Adenosylmethionine synthetase	EC:2.5.1.6
	K00926	Carbamate kinase	EC:2.7.2.2
	K01652	Acetolactate synthase I/II/III large subunit	EC:2.2.1.6
	K01653	Acetolactate synthase I/III small subunit	EC:2.2.1.6
	K00812	Aspartate aminotransferase	EC:2.6.1.1
	K00611	Ornithine carbamoyltransferase	EC:2.1.3.3
	K00640	Serine *O*-acetyltransferase	EC:2.3.1.30
	K14682	Amino-acid *N*-acetyltransferase	EC:2.3.1.1
	K00052	3-Isopropylmalate dehydrogenase	EC:1.1.1.85
	K00145	*N*-Acetyl-*γ*-glutamyl-phosphate reductase	EC:1.2.1.38
Sulfur metabolism	K01011	Thiosulfate/3-mercaptopyruvate sulfurtransferase	EC:2.8.1.1/2.8.1.2
	K02439	Thiosulfate sulfurtransferase	EC:2.8.1.1
	K15553	Sulfonate transport system substrate-binding protein	-
	K15554	Sulfonate transport system permease protein	-
	K15555	Sulfonate transport system ATP-binding protein	EC:3.6.3.-
	K17218	Sulfide:quinone oxidoreductase	EC:1.8.5.4
	K02048	Sulfate/thiosulfate transport system substrate-binding protein	-
	K02046	Sulfate/thiosulfate transport system permease protein	-
	K02045	Sulfate/thiosulfate transport system ATP-binding protein	EC:7.3.2.3
	K00957	Sulfate adenylyltransferase subunit 2	EC:2.7.7.4
	K00390	Phosphoadenosine phosphosulfate reductase	EC:1.8.4.8 (1.8.4.10)
	K10764	*O*-Succinylhomoserine sulfhydrylase	EC:2.5.1.-
	K01738	Cysteine synthase	EC:2.5.1.47
Carbon metabolism	K18118	Succinyl-CoA:acetate CoA-transferase	EC:2.8.3.18
	K01903	Succinyl-CoA synthetase beta subunit	EC:6.2.1.5
	K01902	Succinyl-CoA synthetase alpha subunit	EC:6.2.1.5
	K00640	Serine *O*-acetyltransferase	EC:2.3.1.30
	K00948	Ribose-phosphate pyrophosphokinase	EC:2.7.6.1
	K00873	Pyruvate kinase	EC:2.7.1.40
	K00627	Pyruvate dehydrogenase E2 component (dihydrolipoamide acetyltransferase)	EC:2.3.1.12
	K00163	Pyruvate dehydrogenase E1 component	EC:1.2.4.1
	K01960	Pyruvate carboxylase subunit B	EC:6.4.1.1
	K01959	Pyruvate carboxylase subunit A	EC:6.4.1.1
	K01690	Phosphogluconate dehydratase	EC:4.2.1.12
	K01595	Phosphoenolpyruvate carboxylase	EC:4.1.1.31
	K13788	Phosphate acetyltransferase	EC:2.3.1.8
	K01638	Malate synthase	EC:2.3.3.9
	K01637	Isocitrate lyase	EC:4.1.3.1
	K00031	Isocitrate dehydrogenase	EC:1.1.1.42

Table 2 (*Continued*)

Function	KO	KO function	Enzyme
Carbon metabolism	K00600	Glycine hydroxymethyltransferase	EC:2.1.2.1
	K00281	Glycine dehydrogenase	EC:1.4.4.2
	K00018	Glycerate dehydrogenase	EC:1.1.1.29
	K00134	Glyceraldehyde 3-phosphate dehydrogenase	EC:1.2.1.12
	K00036	Glucose-6-phosphate 1-dehydrogenase	EC:1.1.1.49 (1.1.1.363)
	K00851	Gluconokinase	EC:2.7.1.12
	K00845	Glucokinase	EC:2.7.1.2
	K01679	Fumarate hydratase, class II	EC:4.2.1.2
	K01676	Fumarate hydratase, class I	EC:4.2.1.2
	K00382	Dihydrolipoamide dehydrogenase	EC:1.8.1.4
	K01647	Citrate synthase	EC:2.3.3.1
	K03781	Catalase	EC:1.11.1.6
	K00605	Aminomethyltransferase	EC:2.1.2.10
	K00249	Acyl-coenzyme A dehydrogenase	EC:1.3.8.7
	K01681	Aconitate hydratase	EC:4.2.1.3
	K01057	6-Phosphogluconolactonase	EC:3.1.1.31
	K00033	6-Phosphogluconate dehydrogenase	EC:1.1.1.44 (1.1.1.343)
	K00658	2-Oxoglutarate dehydrogenase E2 component (dihydrolipoamide succinyltransferase)	EC:2.3.1.61
	K00164	2-Oxoglutarate dehydrogenase E1 component	EC:1.2.4.2
	K00874	2-Dehydro-3-deoxygluconokinase	EC:2.7.1.45

Note: - Indicates the EC number is lacking.

close relationship between genes and spoilage volatiles is warranted. The genes involving in amino acid metabolism and carbon metabolism were listed in Table 2 to provide reference. Among them, the gene encoding acetolactate synthase was known as a contributor of diacetyl production[23]. Additionally, sulfur metabolism was another important metabolic pathway that was responsible for the *P. fragi* induced pungent odors associated with S-compounds in beef[5,18]. As shown in Table 2, some genes annotated to sulfur metabolism were found in the *P. fragi* T1 genome, such as sulfate/thiosulfate transport system substrate-binding protein, sulfate/thiosulfate transport system permease protein, sulfate/thiosulfate transport system ATP-binding protein, sulfate adenylyltransferase subunit 2, and cysteine synthase, etc., suggesting that *P. fragi* T1 had certain potential in the sulfur metabolism.

Putrescine is the main biogenic amines (BAs) from spoiled meat[24]. In this study, several genes encoding putrescine transport system ATP-binding protein, putrescine transport system permease protein, and putrescine transport system substrate-binding protein were found in the *P. fragi* T1 genome. In addition, the gene that encodes ornithine decarboxylase was found in the *P. fragi* T1 genome, and this enzyme catalyzed the putrescine production from ornithine[24]. Although some studies suggested that the production of BAs by *Pseudomonas* was strain-dependent[25–26], the above results in the present study proved that *P. fragi* T1 may indeed release putrescine.

3.2 Changes in VOCs production

A total of 11 VOCs was identified during storage. They were diacetyl, (*E*)-2-octenal, 2-undecanone, (*Z*)-5-decen-1-ol, 1-undecene, decanal, hexanoic acid ethyl ester, acetic acid hexyl ester, nonanal, acetic acid, and octanoic acid ethyl ester, respectively. The heatmap clearly visualized the differences in samples during storage based on VOCs concentration and variety. Obviously, the samples of C-8d and C-12d were varied with other samples, indicating the concentration and diversity of VOCs in CMAP samples may undergo a transformation after day 8 (Figure 2A).

Packaging, inoculation type, and storage time interacted to impact the levels of diacetyl, (*Z*)-5-decen-1-ol, 1-undecene, 2-undecanone, and (*E*)-2-octenal (Table 3). There was no diacetyl, (*Z*)-5-decen-1-ol, 1-undecene, or (*E*)-2-octenal detected in the samples stored under TMAP, Blank-TMAP, and Blank-CMAP. This was resulted from the superior antibacterial effect of CO_2 on bacterial growth and related bacterial metabolic activities. The presence of CO_2 demonstrated a distinguished inhibitory effect on *P. fragi* growth, with *P. fragi* counts in TMAP samples always maintaining at approximately 5 (lg (CFU/mL)) throughout the entire storage ($P > 0.05$). Conversely, CMAP samples exhibited a significantly increased *P. fragi* count ($P < 0.05$) over time, and the bacterial count reached 9.02 (lg (CFU/mL)) on day 8 and then entered a stable phase (data not shown). With the extension of storage, the levels of diacetyl, (*Z*)-5-decen-1-ol, 1-undecene, and 2-undecanone significantly increased ($P < 0.05$) in CMAP samples inoculated with *P. fragi* and reached the highest concentration on day 12, in which diacetyl and (*E*)-2-octenal were only detected on day 12. Diacetyl is an important volatile compound contributing to the development of butter-like off-odor in beef samples under aerobic storage, which is related to the growth of *P. fragi*[7–8,18,27]. In the results of genome sequencing, the gene related to acetolactate synthase was detected (Table 2). Moreover, numerous studies found (*E*)-2-octenal was a *Pseudomonas*-related volatile compound in meat[7,28], which was responsible for oily, fatty, and nut odor[29–30]. Stanborough et al.[31] found that 1-undecene was produced by certain *P. fragi* isolates, and it could be used as a marker compound for acceptability/degree of meat spoilage[32]. 1-Undecene could also be used as an aerial communication signal for *P. fluorescens*, and was positively associated with biofilm maturation capacity[33–34]. 2-Undecanone has been shown to possess antibacterial activities[35].

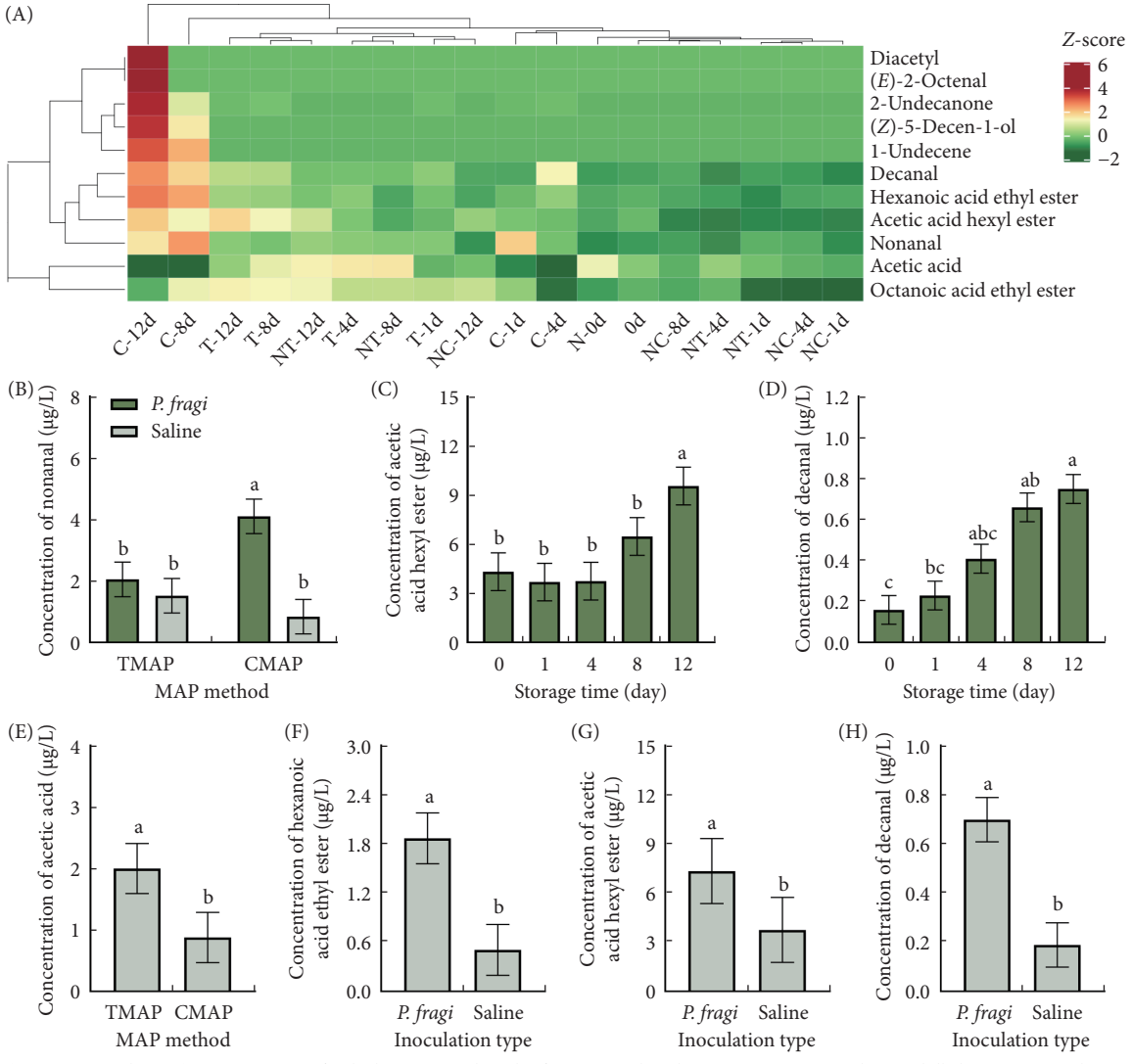

Figure 2 (A) Heatmap and (B–H) concentration of volatile compounds in beef juice stored under two MAP systems during chilled storage. T and C are defined as TMAP (50% O_2/ 40% CO_2/10% N_2) and CMAP (50% O_2/50% N_2), respectively. NT and NC are defined as Blank-TMAP and Blank-CMAP inoculated with 0.85 g/100 mL sterile physiological saline, respectively. Samples are labeled according to storage time (0, 1, 4, 8, and 12 d). Different lowercase letters indicate significant differences between groups ($P < 0.05$).

Table 3 Changes in volatile compounds (μg/L) of beef juice stored under both MAP systems during chilled storage.

Compounds	Packaging	Inoculation type	Storage time (day)					Standard error	*P* value
			0	1	4	8	12		
Diacetyl	TMAP	*P. fragi*						0.32	< 0.001
		Saline							
	CMAP	*P. fragi*					4.41		
		Saline							
(*Z*)-5-Decen-1-ol	TMAP	*P. fragi*						0.41	0.010
		Saline							
	CMAP	*P. fragi*				1.57^{b}	3.44^{a}		
		Saline							
1-Undecene	TMAP	*P. fragi*						1.37	< 0.001
		Saline							
	CMAP	*P. fragi*				28.52^{b}	39.59^{a}		
		Saline							
2-Undecanone	TMAP	*P. fragi*		0.20^{a}		0.30^{a}	0.15^{a}	0.67	0.029
		Saline							
	CMAP	*P. fragi*		0.11^{b}	0.18^{b}	1.68^{b}	5.33^{a}		
		Saline							
(*E*)-2-Octenal	TMAP	*P. fragi*						0.10	0.048
		Saline							
	CMAP	*P. fragi*					0.68		
		Saline							

Note: Different superscript lowercase letters indicate significant differences between storage times ($P < 0.05$). TMAP: 50% O_2/40% CO_2/10% N_2; CMAP: 50% O_2/50% N_2.

However, the role of volatiles in information molecules during meat spoilage is unclear.

Neither inoculation type nor packaging has any effect on the levels of octanoic acid ethyl ester. Inoculation type and packaging interacted to affect nonanal concentrations (Figure 2B). The levels of nonanal in CMAP samples inoculated with *P. fragi* were significantly higher ($P < 0.05$) than those in other treated samples. The storage time had an influence on acetic acid hexyl ester and decanal concentrations (Figures 2C and D), and the concentrations of both volatiles significantly increased on day 12 and day 8 compared to the initial storage phase ($P < 0.05$), respectively. Only the main effect of packaging affected acetic acid concentration. TMAP samples had significantly higher ($P < 0.05$) acetic acid concentrations than CMAP samples (Figure 2E). In addition, the main effect of inoculation type significantly affected hexanoic acid ethyl ester, acetic acid hexyl ester, and decanal concentrations, and *P. fragi* growth caused more three volatiles above than samples inoculated with saline (Figures 2F–H). These volatiles could bring meat sweet fruity odor, such as pear, pineapple, and orange[18], which was consistent with the lipase and esterase activity genes identified in *P. fragi* T1 (Table 2).

3.3 Metabolome analysis of *P. fragi*

3.3.1 *Global analysis of metabolomic response of P. fragi*

The identified metabolites were subjected to OPLS-DA (Figure 3). It was found that 6 replicates from each group were clearly clustered together, while different groups were distinctly separated, as well as QC samples. This indicated good reproducible tests in the same group and sufficient separability among different groups, revealing CO_2 caused the obvious changes in the concentrations and varieties of intracellular metabolites during chilled storage. A total of 35 DEMs was identified in this study, and the heatmap (Figure 4) provided an intuitive visualization of the changes in these metabolite levels. In accordance with the OPLS-DA, the heatmap also indicated that there were various actions of CO_2 against *P. fragi* with the extension of CO_2-treatment.

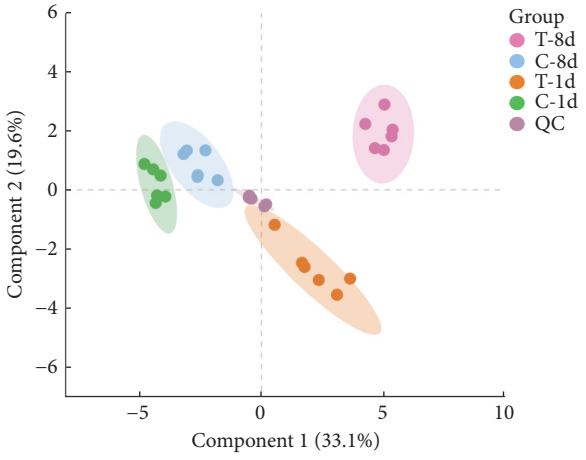

Figure 3 OPLS-DA plot of identified metabolites in *P. fragi* under both MAP methods during chilled storage. T and C are defined as TMAP (50% O_2/40% CO_2/10% N_2) and CMAP (50% O_2/50% N_2), respectively. Samples are labeled according to storage time (1 and 8 d).

KEGG enrichment analysis was carried out to discover the underlying biological alternations in *P. fragi* T1 under CO_2 treatment during storage. The DEMs caused by CO_2 treatment were mainly annotated to the pathways of biosynthesis of amino

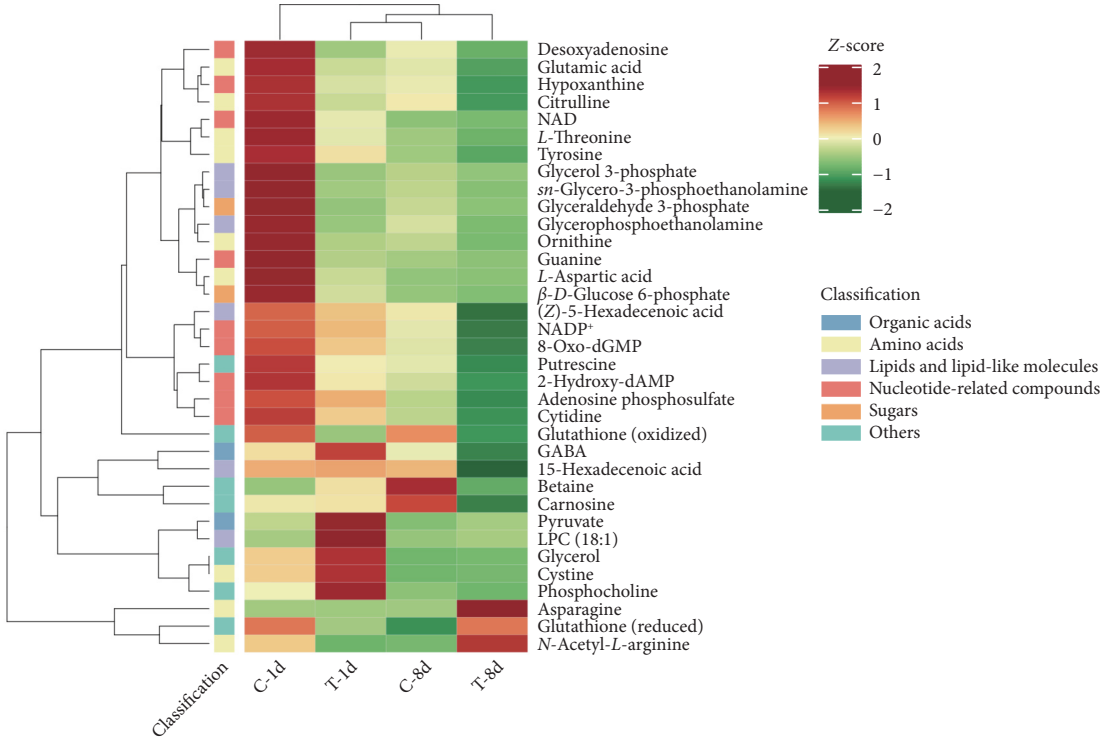

Figure 4 Heatmap of DEMs in *P. fragi* under both MAP methods during chilled storage. T and C are defined as TMAP (50% O_2/40% CO_2/10% N_2) and CMAP (50% O_2/50% N_2), respectively. Samples are labeled according to storage time (1 and 8 d). NAD, nicotinamide adenine dinucleotide; $NADP^+$, oxidized nicotinamide adenine dinucleotide phosphate; GABA, γ-aminobutyrate; LPC, lysophosphatidylcholine.

acids, glycine, serine and threonine metabolism, alanine, aspartate and glutamate metabolism, *D*-amino acid metabolism, pentose phosphate pathway, glycolysis/gluconeogenesis, arginine biosynthesis, arginine and proline metabolism, glycerophospholipid metabolism, citrate cycle (tricarboxylic acid (TCA) cycle), glycerolipid metabolism, glutathione metabolism, pyruvate metabolism, purine metabolism, *β*-alanine metabolism, butanoate metabolism, and histidine metabolism (Figure 5).

3.3.2 *Changes in metabolic process of P. fragi under CO_2 treatment*

3.3.2.1 *Decrease in membrane fluidity*

Bacterial membrane is generally an important target coming from different antibacterial measures[15,36]. A remarkable reduction in the levels of bacterial phospholipids such as phosphocholine in groups of T-8d vs. C-8d and T-8d vs. T-1d, as well as glycerophosphoethanolamine and *sn*-glycerol-3-phosphoethanolamine was observed in groups of T-1d vs. C-1d, T-8d vs. C-8d, T-8d vs. T-1d, and C-8d vs. C-1d (Figure 6), and the absolute value of FC in C-8d vs. C-1d was lower than other three comparison groups. As a small haptenic molecule, phosphocholine is the precursor metabolite of choline in the glycine, serine, and threonine metabolism pathway, and it is also an intermediate between cytidine diphosphatecholine and choline in the glycerophospholipid metabolism pathway[37]. The significantly decreased levels of phosphocholine in the group of T-8d vs. C-8d (Figure 6B) also mean a CO_2-induced disruption in *P. fragi* membrane fluidity due to lipid peroxidation[37]. As we know, fatty acids are important metabolic energy sources and the basic cell membrane components for bacteria[38]. In this study, the concentrations of unsaturated fatty acids including 15-hexadecenoic acid and (*Z*)-5-hexadecenoic acid were down-regulated in both T-1d vs. C-1d and T-8d vs. C-8d (Figures 6A and B). The decreased relative percentage of unsaturated fatty acids tended to decrease membrane fluidity. Therefore, it was inferred that CO_2 not only affected the content of membrane lipids but also disturbed the fatty acid composition, leading to a decrease in membrane fluidity. Jones et al.[39] stated that the two forms of CO_2 have different sites of action upon the cell membrane with CO_2 (aqueous) exerting its effect on the fluidity of the hydrophobic fatty acid core of the membrane, and HCO_3^- exerting its effect on the charged phospholipid head groups and proteins at the surface of the membrane. In support, Kolbeck et al.[40] also detected a decreasing membrane fluidity of *Carnobacterium maltaromaticum* TMW2.1581 in response to CO_2 by changing its membrane fatty acid profiles.

It was worth noting that there were significant positive correlations between glycerophosphoethanolamine, *sn*-glycerol-3-phosphoethanolamine and nonanal (Figure 7). Glycerophosphoethanolamine and *sn*-glycerol-3-phosphoethanolamine were the major lipid fractions in the glycerophospholipid, hinting glycerophospholipid metabolism was associated with the aldehydes formation. The lower contents of nonanal in TMAP samples (Figure 2B) may be due to the inhibitory effect of CO_2 on *P. fragi* glycerophospholipid metabolism.

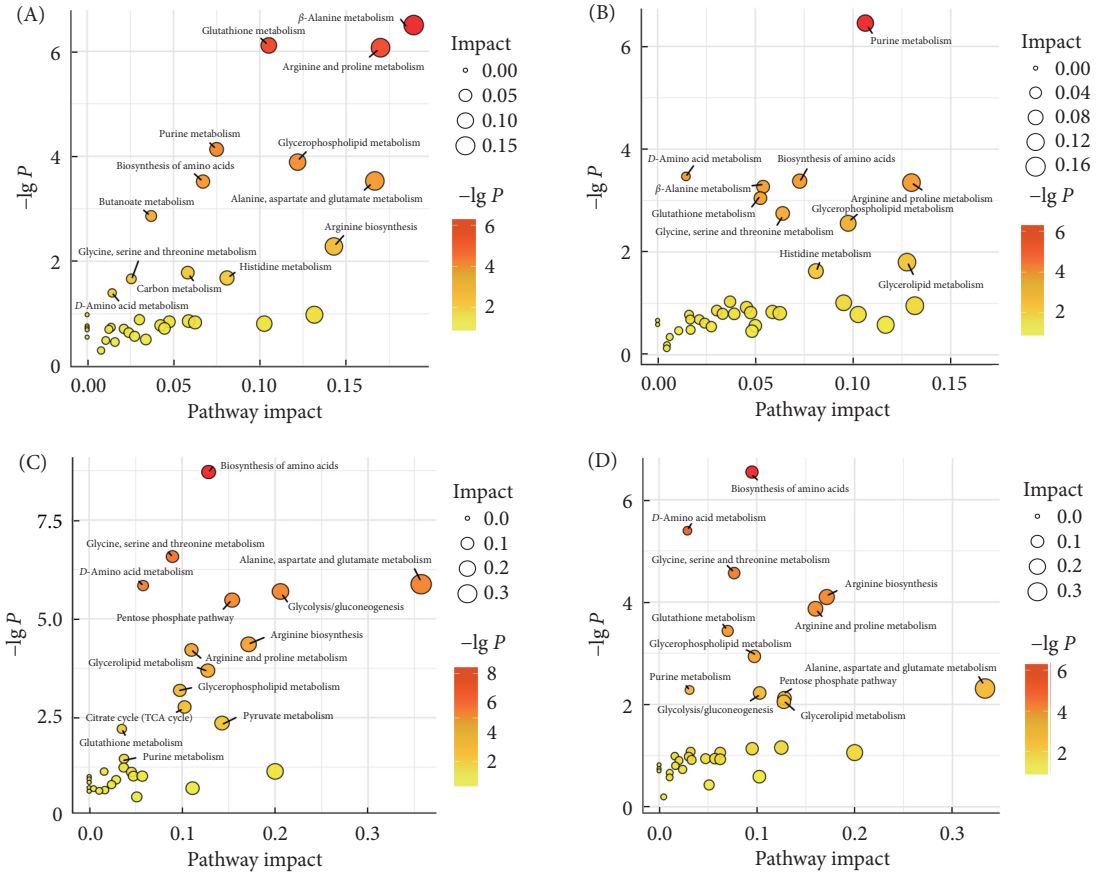

Figure 5 KEGG analysis of DEMs in *P. fragi* under both MAP methods during chilled storage. (A) T-1d vs. C-1d, (B) T-8d vs. C-8d, (C) T-8d vs. T-1d, and (D) C-8d vs. C-1d. T and C are defined as TMAP (50% O_2/40% CO_2/10% N_2) and CMAP (50% O_2/50% N_2), respectively.

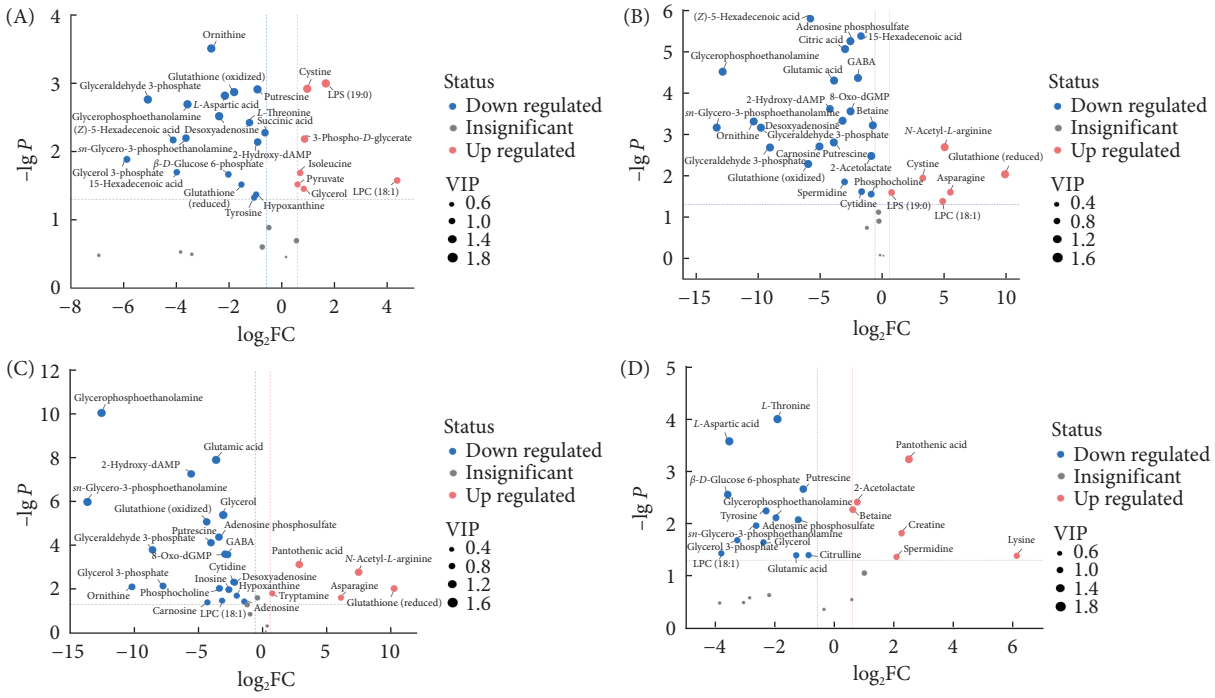

Figure 6 Volcano plots of DEMs in *P. fragi* under both MAP methods during chilled storage. (A) T-1d vs. C-1d, (B) T-8d vs. C-8d, (C) T-8d vs. T-1d, and (D) C-8d vs. C-1d. T and C are defined as TMAP (50% O_2/40% CO_2/10% N_2) and CMAP (50% O_2/50% N_2), respectively. LPS, lipopolysaccharide.

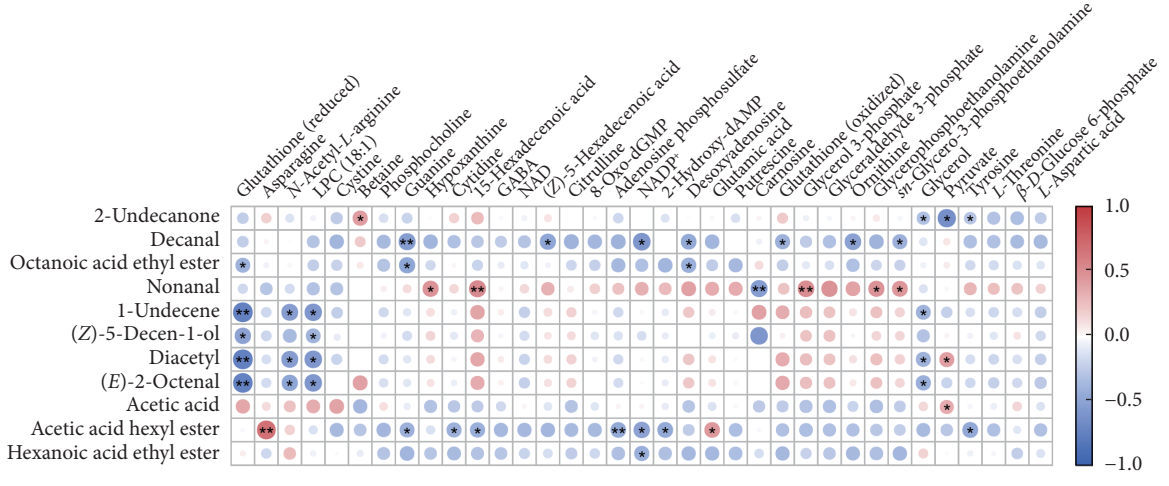

Figure 7 Spearman's correlation between the *P. fragi* DEMs and volatile compounds.

3.3.2.2 *Disturbing energy metabolism*

The TCA cycle is central to energy production and biosynthetic precursor synthesis in aerobic organisms. In this study, succinic acid and citric acid levels were observed to decrease in the groups of T-1d vs. C-1d and T-8d vs. C-8d (Figures 6A and B), respectively. Additionally, the increased pyruvate contents were detected at the initial CO_2-treated stage (Figure 6A). These indicated that CO_2 may disorder bacterial energy metabolism. Additionally, pyruvate was positively correlated with the VOCs of diacetyl and acetic acid as a precursor (Figure 7). Therefore, the higher contents of acetic acid (Figure 2E) were obtained under TMAP than under CMAP may be attributed to the higher pyruvate contents in TMAP. In glycolysis/gluconeogenesis, glyceraldehyde 3-phosphate levels decreased in the groups of T-1d vs. C-1d, T-8d vs. C-8d, and T-8d vs. T-1d (Figures 6A–C), which may inhibit reduced nicotinamide adenine dinucleotide and ATP generation. Li et al.[41] and Wang et al.[42] also demonstrated that CO_2 declined the ATP contents of *S. putrefaciens* and *P. fragi*, respectively.

3.3.2.3 *Inhibiting nucleotide biosynthesis*

The levels of cytidine, 8-oxo-dGMP, adenosine phosphosulfate, 2-hydroxy-dAMP, and desoxyadenosine showed decreasing trends in the both groups of T-8d vs. C-8d and T-8d vs. T-1d (Figures 6B and C). Among them, the levels of 2-hydroxy-dAMP and desoxyadenosine also decreased at the initial CO_2-treated stage (Figure 6A). Additionally, inosine contents declined in the group of T-8d vs. C-1d (Figure 6C). These metabolites are of great importance in the biosynthesis of nucleotides. For example, cytidine nucleotides participate in the feedback regulation of *de novo* synthesis of uridine triphosphate[43]. The nucleoside inosine is an essential metabolite for purine biosynthesis and degradation; it also

acts as a bioactive molecule that regulates RNA editing, metabolic enzyme activity, and signaling pathways[44]. Therefore, it can be reasonably deduced that the presence of CO_2 may have an adverse effect on the *de novo* synthesis of nucleotides.

3.3.2.4 Regulating amino acid metabolism

Amino acid metabolism was classified into the primary function of *P. fragi* T1, and was also susceptible to external stress[15,36]. In this study, the ornithine contents decreased at the initial CO_2-treated stage (Figure 6A). With the extension of CO_2-treatment, the levels of ornithine, putrescine, and GABA decreased in the groups of T-8d vs. C-8d and T-8d vs. T-1d (Figures 6B and C), indicating the restrictive effect of CO_2 was more pronounced in the late stage than in the initial stage. Putrescine is a meat spoilage index that is caused by microbial decarboxylation reaction of ornithine activity[24]. According to the previous reviews[10], CO_2 inhibited some certain decarboxylation enzymes activities. Therefore, the reduction in putrescine levels also demonstrated that CO_2 diminished the metabolic activity related to *P. fragi* putrescine metabolism, which may thereby delay the increased pH and TVB-N content in ground beef under the same modified atmospheres, and help retain meat freshness due to the putrescine reduction[8,45]. Furthermore, putrescine is a precursor to GABA[46]. The reduction of putrescine also explained the decrease in GABA in T-8d vs. C-8d and T-8d vs. T-1d.

There were strong positive correlations between acetic acid hexyl ester and asparagine and glutamic acid (Figure 7). Similarly, dos Santos et al.[47] reported that aspartate, asparagine, and glutamic acid positively influenced the production of esters in the ciders. However, asparagine and glutamic acid exhibited distinct expression patterns in response to CO_2 in this study (Figures 6B and C). Accordingly, further investigation is required to ascertain the impact of CO_2 on acetic acid hexyl ester, particularly when samples subjected to two MAP methods exhibit identical colony counts.

3.3.2.5 Inducing oxidative stress and maintaining intracellular homeostasis

The exposure to CO_2 could induce oxidative stress, potentially resulting in the indiscriminate damage of metabolites, nucleic acids, enzymes, and lipids through peroxidation, which could cause several metabolic errors[48–49]. Oxidative stress also destroys the intracellular redox equilibrium of glutathione disulphide redox couples, producing cytotoxicity. Thus, both reduced glutathione (GSH) and oxidized glutathione (GSSG) were down-regulated in the group of T-1d vs. C-1d (Figure 6A). In this process of oxidative stress, glutathione plays a critical role in balancing redox reactions. At the late CO_2-treatment stage, the contents of GSH increased, but GSSG levels declined (Figures 6B and C). And there were no differences in the contents of GSH or GSSG in the control group C-8d vs. C-1d (Figure 6D). GSH is a common antioxidant and free radical scavenger *in vivo*, scavenging reactive oxygen species (ROS) in the process of conversion to GSSG. Armstrong et al.[50] found that the decrease of GSH content was a potential early activation signal of apoptosis, and the subsequent generation of ROS can promote cell apoptosis. The observed increase in GSH levels and the decrease in GSSG levels suggested that the capacity of *P. fragi* to resist oxidative stress was enhanced by the stimulation of CO_2, which may further eliminate intracellular ROS accumulation. Besides, the glutamic acid levels demonstrated a declined tendency in the group of T-8d vs. C-8d, which may be attributed to the production of glutathione to maintain the redox reaction equilibrium[51]. Cysteine was reported as the rate-limiting amino acid for glutathione synthesis[52–53], and its increased contents in T-8d vs. C-8d were consistent with the increased concentrations of GSH (Figure 6B).

4 Conclusion

This study identified that the wild-type *P. fragi* T1 with strong meat spoilage potential had genes involving amino acid metabolism, carbon metabolism, sulfur metabolism, putrescine metabolism, protease, lipase, and esterase production, which contributed to meat spoilage process. Meanwhile, *P. fragi* T1 possessed plenty of genes participating in two-component systems and ABC transporters, hinting this strain also presented the ability to resist CO_2. CO_2 inhibited the *P. fragi* growth, and reduced the VOCs concentrations (e.g., diacetyl, 1-undecene, 2-undecanone, nonanal, (*Z*)-5-decen-1-ol, and (*E*)-2-octenal, etc.) by decreasing cell membrane fluidity, disturbing energy metabolism, and inhibiting amino acid metabolism and nucleotide biosynthesis. This work will be useful for identifying potential targets for developing meat processing strategies to achieve more effective control of *P. fragi*. It is of critical and urgent importance to decipher the regulatory effect of CO_2 on key metabolic targets associated with primary VOCs formation in future work.

Conflict of interest

The authors declare that they have no known competing financial interests or personal relationships that could have appeared to influence the work reported in this paper.

Acknowledgements

This work was supported by the Projects of National Natural Science Foundation of China (32372409), the Earmarked Fund for China Agriculture Research System of Ministry of Finance and Ministry of Agriculture and Rural Affairs (CARS-37), and Special Funds for the Central Government to Guide Local Science and Technology Development (YDZX2022149).

References

[1] X. Y. Yang, L. X. Zhu, Y. M. Zhang, et al., Microbial community dynamics analysis by high-throughput sequencing in chilled beef *longissimus* steaks packaged under modified atmospheres, Meat Sci. 141 (2018) 94–102. https://doi.org/10.1016/j.meatsci.2018.03.010.

[2] J. Yang, X. Y. Yang, R. R. Liang, et al., The response of bacterial communities to carbon dioxide in high-oxygen modified atmosphere packaged beef steaks during chilled storage, Food Res. Int. 151 (2022) 110872. https://doi.org/10.1016/j.foodres.2021.110872.

[3] X. Y. Yang, X. Luo, Y. M. Zhang, et al., Effects of microbiota dynamics on the color stability of chilled beef steaks stored in high oxygen and carbon monoxide packaging, Food Res. Int. 134 (2020) 109215. https://doi.org/10.1016/j.foodres.2020.109215.

[4] J. Yang, X. Y. Yang, H. Lin, et al., Investigation of the relationship between microbiota dynamics and volatile changes in chilled beef steaks held under high-oxygen packaging enriched in carbon dioxide, Meat Sci. 191 (2022) 108861. https://doi.org/10.1016/j.meatsci.2022.108861.

[5] D. Ercolini, A. Casaburi, A. Nasi, et al., Different molecular types of *Pseudomonas fragi* have the same overall behaviour as meat

spoilers, Int. J. Food Microbiol. 142 (2010) 120–131. https://doi.org/10.1016/j.ijfoodmicro.2010.06.012.

[6] N. N. Wickramasinghe, J. Ravensdale, R. Coorey, et al., The predominance of psychrotrophic pseudomonads on aerobically stored chilled red meat, Compr. Rev. Food Sci. Food Saf. 18 (2019) 1622–1635. https://doi.org/10.1111/1541-4337.12483.

[7] O. S. Papadopoulou, V. Iliopoulos, A. Mallouchos, et al., Spoilage potential of *Pseudomonas* (*P. fragi*, *P. putida*) and LAB (*Leuconostoc mesenteroides*, *Lactobacillus sakei*) strains and their volatilome profile during storage of sterile pork meat using GC/MS and data analytics, Foods 9(5) (2020) 633. https://doi.org/10.3390/foods9050633.

[8] J. Yang, R. R. Liang, Y. W. Mao, et al., Potential inhibitory effect of carbon dioxide on the spoilage behaviors of *Pseudomonas fragi* in high-oxygen packaged beef during refrigerated storage, Food Microbiol. 112 (2023) 104229. https://doi.org/10.1016/j.fm.2023.104229.

[9] X. Y. Yang, L. B. Niu, L. X. Zhu, et al., Shelf-life extension of chill-stored beef *longissimus* steaks packaged under modified atmospheres with 50% O_2 and 40% CO_2, J. Food Sci. 81 (2016) C1692–C1698. https://doi.org/10.1111/1750-3841.13345.

[10] J. A. Daniels, R. Krishnamurthi, S. S. H. Rizvi, A review of effects of carbon dioxide on microbial growth and food quality, J. Food Prot. 48 (1985) 532–537. https://doi.org/10.4315/0362-028X-48.6.532.

[11] J. M. Farber, Microbiological aspects of modified atmosphere packaging technology: a review, J. Food Prot. 54 (1991) 58–70. https://doi.org/10.4315/0362-028X-54.1.58.

[12] W. H. Oliver, The effect of carbon dioxide pressure on a bacterial decarboxylase system, Microbiology 8 (1953) 38–44. https://doi.org/10.1099/00221287-8-1-38.

[13] A. D. King Jr., C. W. Nagel, Influence of carbon dioxide upon the metabolism of *Pseudomonas aeruginosa*, J. Food Sci. 40 (1975) 362–366. https://doi.org/10.1111/j.1365-2621.1975.tb02202.x.

[14] K. H. Tan, C. O. Gill, Physiological basis of CO_2 inhibition of a meat spoilage bacterium, *Pseudomonas fluorescens*, Meat Sci. 7 (1982) 9–17. https://doi.org/10.1016/0309-1740(82)90093-6.

[15] Z. L. Tang, H. M. Chen, W. J. Chen, et al., Unraveling the antibacterial mechanism of 3-carene against *Pseudomonas fragi* by integrated proteomics and metabolomics analyses and its application in pork, Int. J. Food Microbiol. 379 (2022) 109846. https://doi.org/10.1016/j.ijfoodmicro.2022.109846.

[16] Y. S. Li, R. R. He, H. M. Chen, et al., Respiratory depression as antibacterial mechanism of linalool against *Pseudomonas fragi* based on metabolomics, Int. J. Mol. Sci. 23 (2022) 11586. https://doi.org/10.3390/ijms231911586.

[17] N. Illikoud, R. Gohier, D. Werner, et al., Transcriptome and volatilome analysis during growth of *Brochothrix thermosphacta* in food: role of food substrate and strain specificity for the expression of spoilage functions, Front. Microbiol. 10 (2019) 2527. https://doi.org/10.3389/fmicb.2019.02527.

[18] A. Casaburi, P. Piombino, G. J. Nychas, et al., Bacterial populations and the volatilome associated to meat spoilage, Food Microbiol. 45 (2015) 83–102. https://doi.org/10.1016/j.fm.2014.02.002.

[19] R. Colin, B. Ni, L. Laganenka, et al., Multiple functions of flagellar motility and chemotaxis in bacterial physiology, FEMS Microbiol. Rev. 45 (2021) fuab038. https://doi.org/10.1093/femsre/fuab038.

[20] G. J. Nychas, C. C. Tassou, Spoilage processes and proteolysis in chicken as detected by HPLC, J. Sci. Food Agric. 74 (1997) 199–208. https://doi.org/10.1002/(SICI)1097-0010(199706)74:2<199::AIDJSFA790>3.0.CO;2-4.

[21] N. Izuchukwu, Production of extracellular proteases by *Aeromonas*, *Serratia* and *Shewanella* species and characterization of extracellular proteases using zymogram analysis, J. Pharm. Biol. Sci. 12 (2017) 42–49. https://doi.org/10.9790/3008-1205074249.

[22] L. Kulakova, A. Galkin, T. Kurihara, et al., Cold-active serine alkaline protease from the psychrotrophic bacterium *Shewanella* strain Ac10: gene cloning and enzyme purification and characterization, Appl. Environ. Microbiol. 65 (1999) 611–617. https://doi.org/10.1128/AEM.65.2.611-617.1999.

[23] M. Andreevskaya, P. Johansson, P. Laine, et al., Genome sequence and transcriptome analysis of meat-spoilage-associated lactic acid bacterium *Lactococcus piscium* MKFS47, Appl. Environ. Microbiol. 81 (2015) 3800–3811. https://doi.org/10.1080/09583157.2019.1657067.

[24] L. Wunderlichová, L. Buňková, M. Koutný, et al., Formation, degradation, and detoxification of putrescine by foodborne bacteria: a review, Compr. Rev. Food Sci. Food Saf. 13 (2014) 1012–1030. https://doi.org/10.1111/1541-4337.12099.

[25] I. Geornaras, G. A. Dykes, A. von Holy, Biogenic amine formation by poultry-associated spoilage and pathogenic bacteria, Lett. Appl. Microbiol. 21 (1995) 164–166. https://doi.org/10.1111/j.1472-765X.1995.tb01032.x.

[26] Y. Y. Ge, J. L. Zhu, X. F. Ye, et al., Spoilage potential characterization of *Shewanella* and *Pseudomonas* isolated from spoiled large yellow croaker (*Pseudosciaena crocea*), Lett. Appl. Microbiol. 64 (2017) 86–93. https://doi.org/10.1111/lam.12687.

[27] C. Franke, L. Höll, H. C. Langowski, et al., Sensory evaluation of chicken breast packed in two different modified atmospheres, Food Packag. Shelf Life 13 (2017) 66–75. https://doi.org/10.1016/j.fpsl.2017.07.005.

[28] F. F. Parlapani, D. A. Anagnostopoulos, E. Karamani, et al., Growth and volatile organic compound production of *Pseudomonas* fish spoiler strains on fish juice agar model substrate at different temperatures, Microorganisms 11 (2023) 189. https://doi.org/10.3390/microorganisms11010189.

[29] J. C. Zhu, F. Chen, L. Y. Wang, et al., Characterization of the key aroma volatile compounds in cranberry (*Vaccinium macrocarpon* Ait.) using gas chromatography-olfactometry (GC-O) and odor activity value (OAV), J. Agric. Food Chem. 64 (2016) 4990–4999. https://doi.org/10.1021/acs.jafc.6b01150.

[30] Q. Y. Guo, J. W. Yu, Y. Y. Zhao, et al., Identification of fishy odor causing compounds produced by *Ochromonas* sp. and *Cryptomonas ovate* with gas chromatography-olfactometry and comprehensive two-dimensional gas chromatography, Sci. Total Environ. 671 (2019) 149–156. https://doi.org/10.1016/j.scitotenv.2019.03.370.

[31] T. Stanborough, N. Fegan, S. M. Powell, et al., Genomic and metabolic characterization of spoilage-associated *Pseudomonas* species, Int. J. Food Microbiol. 268 (2018) 61–72. https://doi.org/10.1016/j.ijfoodmicro.2018.01.005.

[32] R. H. Dainty, R. A. Edwards, C. M. Hibbard, Volatile compounds associated with the aerobic growth of some *Pseudomonas* species on beef, J. Appl. Bacteriol. 57 (1984) 75–81. https://doi.org/10.1111/j.1365-2672.1984.tb02358.x.

[33] C. A. Dupont, Y. Bourigault, T. Osmond, et al., *Pseudomonas fluorescens* MFE01 uses 1-undecene as aerial communication molecule, Front. Microbiol. 14 (2023) 1264801. https://doi.org/10.3389/fmicb.2023.1264801.

[34] Z. Rui, X. Li, X. J. Zhu, et al., Microbial biosynthesis of medium-chain 1-alkenes by a nonheme iron oxidase, Proc. Natl. Acad. Sci. 111 (2014) 18237–18242. https://doi.org/10.1073/pnas.1419701112.

[35] A. A. Popova, O. A. Koksharova, V. A. Lipasova, et al., Inhibitory and toxic effects of volatiles emitted by strains of *Pseudomonas* and *Serratia* on growth and survival of selected microorganisms, *Caenorhabditis elegans*, and *Drosophila melanogaster*, Biomed Res. Int. 2014 (2014) 125704. https://doi.org/10.1155/2014/125704.

[36] M. M. Liu, M. X. Feng, K. Yang, et al., Transcriptomic and metabolomic analyses reveal antibacterial mechanism of astringent

persimmon tannin against methicillin-resistant *Staphylococcus aureus* isolated from pork, Food Chem. 309 (2020) 125692. https://doi.org/10.1016/j.foodchem.2019.125692.

[37] B. Y. Zeng, M. H. Su, Q. X. Chen, et al., *Anoectochilus roxburghii* polysaccharide prevents carbon tetrachloride-induced liver injury in mice by metabolomic analysis, J. Chromatogr. B 1152 (2020) 122202. https://doi.org/10.1016/j.jchromb.2020.122202.

[38] P. Schönfeld, L. Wojtczak, Short- and medium-chain fatty acids in energy metabolism: the cellular perspective, J. Lipid Res. 57 (2016) 943–954. https://doi.org/10.1194/jlr.R067629.

[39] R. P. Jones, P. F. Greenfield, Effect of carbon dioxide on yeast growth and fermentation, Enzyme Microb. Technol. 4 (1982) 210–223. https://doi.org/10.1016/0141-0229(82)90034-5.

[40] S. Kolbeck, H. Kienberger, K. Kleigrewe, et al., Effect of high levels of CO_2 and O_2 on membrane fatty acid profile and membrane physiology of meat spoilage bacteria, Eur. Food Res. Technol. 247 (2021) 999–1011. https://doi.org/10.1007/s00217-020-03681-y.

[41] P. Y. Li, J. Mei, J. Xie, Carbon dioxide can inhibit biofilms formation and cellular properties of *Shewanella putrefaciens* at both 30 °C and 4 °C, Food Res. Int. 161 (2022) 111781. https://doi.org/10.1016/j.foodres.2022.111781.

[42] G. Y. Wang, F. Ma, L. Y. Zeng, et al., Modified atmosphere packaging decreased *Pseudomonas fragi* cell metabolism and extracellular proteolytic activities on meat, Food Microbiol. 76 (2018) 443–449. https://doi.org/10.1016/j.fm.2018.07.007.

[43] J. Neuhard, Pyrimidine nucleotide metabolism and pathways of thymidine triphosphate biosynthesis in *Salmonella typhimurium*, J. Bacteriol. 96 (1968) 1519–1527. https://doi.org/10.1128/jb.96.5.1519-1527.1968.

[44] I. S. Kim, E. K. Jo, Inosine: a bioactive metabolite with multimodal actions in human diseases, Front. Pharmacol. 13 (2022) 1043970. https://doi.org/10.3389/fphar.2022.1043970.

[45] A. E. D. A. Bekhit, B. W. B. Holman, S. G. Giteru, et al., Total volatile basic nitrogen (TVB-N) and its role in meat spoilage: a review, Trends Food. Sci. Technol. 109 (2021) 280–302. https://doi.org/10.1016/j.tifs.2021.01.006.

[46] J. M. P. Jorge, A. Q. D. Nguyen, F. Pérez-García, et al., Improved fermentative production of γ-aminobutyric acid via the putrescine route: systems metabolic engineering for production from glucose, amino sugars, and xylose, Biotechnol. Bioeng. 114 (2017) 862–873. https://doi.org/10.1002/bit.26211.

[47] C. M. E. dos Santos, A. Alberti, G. D. A. M. Pietrowski, et al., Supplementation of amino acids in apple must for the standardization of volatile compounds in ciders, J. Inst. Brew. 122 (2016) 334–341. https://doi.org/10.1002/jib.318.

[48] G. Piedrafita, M. A. Keller, M. Ralser, The impact of non-enzymatic reactions and enzyme promiscuity on cellular metabolism during (oxidative) stress conditions, Biomolecules 5 (2015) 2101–2122. https://doi.org/10.3390/biom5032101.

[49] B. Ezraty, M. Chabalier, A. Ducret, et al., CO_2 exacerbates oxygen toxicity, EMBO Rep. 12 (2011) 321–326. https://doi.org/10.1038/embor.2011.7.

[50] J. S. Armstrong, D. P. Jones, Glutathione depletion enforces the mitochondrial permeability transition and causes cell death in HL60 cells that overexpress Bcl-2, FASEB J. 16 (2002) 1263–1265. https://doi.org/10.1096/fj.02-0097fje.

[51] M. D. Xie, W. Q. Chen, X. C. Lai, et al., Metabolic responses and their correlations with phytochelatins in *Amaranthus hypochondriacus* under cadmium stress, Environ. Pollut. 252 (2019) 1791–1800. https://doi.org/10.1016/j.envpol.2019.06.103.

[52] R. Dringen, Metabolism and functions of glutathione in brain, Prog. Neurobiol. 62 (2000) 649–671. https://doi.org/10.1016/S0301-0082(99)00060-X.

[53] P. Maher, The effects of stress and aging on glutathione metabolism, Ageing Res. Rev. 4 (2005) 288–314. https://doi.org/10.1016/j.arr.2005.02.005.